NEUTRINO PHYSICS, MASSES, AND OSCILLATIONS

MICHAEL H. SHAEVITZ
COLUMBIA UNIVERSITY
DEPT. OF PHYSICS, NEW YORK, NY 10027

Neutrino physics is reviewed in the context of recent experiments and results. The lectures begin with a brief introduction to neutrino interactions in the Standard Model, and measurement techniques. The NuTeV electroweak measurement is then presented as an example of a precision high energy neutrino experiment. Neutrino properties and mass phenomenology is reviewed, followed by an overview of direct mass measurements. The bulk of the lectures then concentrates on neutrino oscillations. Solar, atmospheric, and high mass experimental measurements are described, compared, and fit into a global context. The conclusion then considers future prospects and speculations.

1 Introduction

Neutrinos hold a special place in the Standard Model because they only interact through the weak force. The interaction is mediated by the exchange of W and Z bosons with only a parity-violating, vector minus axial−vector (V−A) coupling. As a result neutrinos are left-handed and antineutrinos are right-handed. Neutrinos have lepton number associated with their charged-lepton partners, the electron, muon, and tau leptons. For charged-current (W exchange) interactions, an incident neutrino of a given type produces the associated charged lepton type ($\nu_e \to e$, $\nu_\mu \to \mu$, and $\nu_\tau \to \tau$). In the Standard Model, neutrinos are massless since the standard Dirac mass term cannot be included if wrong-handed neutrinos do not exist. Since recent neutrino oscillation measurements show that neutrinos have small masses, the Standard Model must be augmented in some way to explain this.

Historically, the neutrino was first postulated by Pauli to explain energy non-conservation in beta decay. Reines and Cowan[1] observed the first interactions of electron antineutrinos in 1953, for which Reines received the Nobel prize in 1995. Lederman, Schwartz, and Steinberger[2] in 1962 detected muon neutrino interactions showing that neutrinos come in at least two types; they received the Nobel prize for this work in 1988. Evidence for tau neutrino interactions was published in 2000[3], thus filling out the observation of the three neutrinos. In the late 1980's, precision measurements of the invisible Z width by the LEP experiments showed that within the Standard Model there are only three light neutrino types.

Two historical observations are particularly noteworthy. First, the observation of neutrino neutral current interactions was key in establishing the Standard Model and electroweak unification. The second was the recent observation of neutrino oscillations, first proposed by Pontecorvo in 1957. Neutrino oscillations imply massive neutrinos, which is the first indication of physics beyond the Standard Model.

1.1 Neutrino Interactions

Neutrinos interact with quarks and leptons through the charged-current (CC) interaction mediated by W exchange, and the neutral-current (NC) interaction mediated by Z exchange. Neutrinos can scatter off leptons or quarks in nucleons. The point cross section for the scattering is proportional to the (center-of-mass energy)^2, and is given by $\sigma_{tot} = G_F^2 s/\pi\,(\textit{spin-dependent factor})$. To calculate the spin-dependent factor for the charged-current interaction, the V−A nature determines the handedness of the interacting particles; particles need to be left-handed and antiparticles right-handed. The NC interaction is a mixture of V−A and V+A coupling depending on the charge of the particle as given in the following table:

Z Couplings	$V - A = g_L$	$V + A = g_R$
ν_e, ν_μ, ν_τ	$1/2$	0
e, μ, τ	$-1/2 + \sin^2\theta_W$	$\sin^2\theta_W$
u, c, t	$1/2 - 2/3\sin^2\theta_W$	$-2/3\sin^2\theta_W$
d, s, b	$-1/2 + 1/3\sin^2\theta_W$	$1/3\sin^2\theta_W$

The handedness of a particle is not the same thing as its helicity. Helicity is the projection of the particle's spin along the direction of motion, and is Lorentz-frame dependent if the particle is massive. The helicity operator, $\sigma \cdot p$, gives a positive (right) helicity for the spin along the particle's direction and negative (left) for the opposite orientation. On the other hand, the weak interaction V−A and V+A couplings refer to the handedness of the particles. Handedness (or chirality) is Lorentz invariant and is only the same as helicity for massless particles. A massive left-handed particle will be mainly left-helicity but with a small right-helicity component of size $\propto m/E$. Neutrinos only interact weakly with a V−A coupling for both NC and CC interactions, so all neutrinos are left-handed and all antineutrinos are right-handed. If neutrinos are massless, then their helicities are also always left-helicity. But if neutrinos have a small mass, they will be mainly left-helicity with a small ($\propto m_\nu/E_\nu$) right-helicity.

Pure leptonic neutrino scattering is simple theoretically, but hard to investigate experimentally due to the very small cross sections. For the CC inverse-muon-decay process, $\nu_\mu + e^- \rightarrow \mu^- + \nu_e$, a left-handed neutrino interacts with a left-handed electron giving a total spin of zero and an isotropic distribution in the center-of-mass frame. The total cross section for the process is $\sigma_{tot} = G_F^2 s/\pi \cdot (1 - m_\mu^2/s) = 17.2 \times 10^{-42}\mathrm{cm}^2/\mathrm{GeV}\cdot E_\nu \cdot (1 - m_\mu^2/s)$. For NC elastic scattering, $\nu_\mu + e^- \rightarrow \nu_\mu + e^-$, the Z couples to the electron with both a V−A and V+A coupling with the above strengths. The V−A part is the same as the inverse muon decay with a total spin of zero, but the V+A part has a left-handed neutrino interacting with a right-handed electron giving a total spin of one. The total cross section for the elastic scattering process is $\sigma_{tot} = G_F^2 s/\pi \left(\frac{1}{4} - \sin^2\theta_W + \frac{4}{3}\sin^4\theta_W\right)$.

For neutrino-nucleon (proton or neutron) scattering, the target nucleon complicates the process, since it is composed of a collection of quarks and gluons. The total cross section for neutrino-nucleon scattering also rises linearly with s or E_ν^{lab}, but different processes dominate as a function of incident neutrino energy (Fig. 1). At low energy, the neutrino can scatter from the nucleon as a whole through a CC or "quasi-elastic" ($\nu_\mu + n \rightarrow \mu^- + p$) or NC or "elastic" ($\nu_\mu + N \rightarrow \nu_\mu + N$) process. Which process dominates is dependent on the incident neutrino energy and on the four-momentum transfer to the nucleon, $Q^2 \approx \left(4E_\nu E_l \sin^2(\theta/2)\right)_{Lab}$. Above $Q^2 > 1$ GeV^2, the target nucleon can be excited to a Δ or N* resonance (i.e. $\nu_\mu + n \rightarrow \mu^- + \Delta^+ \rightarrow \mu^- + n + \pi^+$ and $\nu_\mu + n \rightarrow \nu_\mu + \Delta^0 \rightarrow \mu^- + n + \pi^0$) which is referred to as "resonance" or single-pion production. At even higher $Q^2 > 5$ GeV^2, the neutrino has the resolution to "see" the constituent quarks, and interactions are dominated by neutrino-quark scattering ($\nu_\mu + q \rightarrow \mu^- + q'$), commonly called "deep-inelastic" scattering. Deep-inelastic scattering is dependent on three variables: E_ν, Q^2, and x. The new variable x is related to the momentum fraction of the struck quark and is given by $x = Q^2/\left(2M(E_\nu - E_l)\right)$. For CC deep-inelastic scattering, the differential cross section is given in terms of the quark form factors of the nucleon called "structure functions"; $\mathrm{F}_2(x) = xq(x) + x\overline{q}(x) =$ the momentum distribution of quarks and anti-quarks and $\mathrm{xF}_3(x) = xu_{val}(x) + xd_{val}(x) =$ momentum distribution of valence quarks in the nucleon. The cross section is then written :

$$\frac{d^2\sigma^{\nu(\overline{\nu})N}}{dx\ dy} = \frac{G_F^2 s}{2\pi}\left((1 + (1-y)^2)F_2(x) \pm (1 - (1-y)^2)xF_3(x)\right)$$

The neutrino cross sections are small due to the exchange of the massive W or Z bosons; the total cross section goes as $(1/M_W)^4$. Phenomenologically, the strength is proportional to the Fermi constant, $G_F = \sqrt{2}/8\,(g_W/M_W)^2 =$

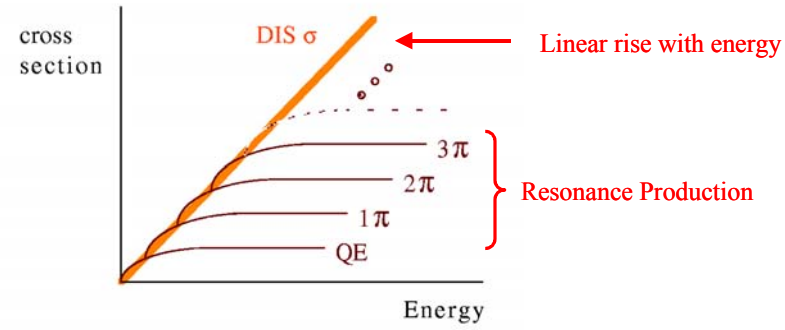

Figure 1. A schematic representation of the neutrino cross section in terms of its components.

$1.166 \times 10^{-5}/GeV^2$ where $g_W \approx 0.7$ is the underlying weak coupling strength and is not small. Quantitatively, the size of the neutrino total cross section at $E_\nu = 100$ GeV is $\sigma(\nu e) \sim 10^{-40}\text{cm}^2$ and $\sigma(\nu N) \sim 10^{-36}\text{cm}^2$ as compared to proton-proton scattering, $\sigma(pp) \sim 10^{-26}\text{cm}^2$. With a cross section this small, neutrinos have a very long mean free path in material ($\sim 3 \times 10^9$ meters in steel) and neutrino experiments therefore need to be very massive.

These lectures cannot cover all of neutrino physics, but will examine two areas of active research. In the next section, the recent NuTeV electroweak measurements will be described as an example of a high energy neutrino scattering experiment. This will be followed by several sections on the neutrino mass phenomenology and experimentation including direct mass and neutrino oscillation experiments. Other topics related to QCD and quark distribution measurements using neutrinos will not be covered but can be found in various review articles[4].

2 Neutrino Electroweak Measurements

Neutrino scattering has played a key role in establishing the structure of the Standard Model of electroweak unification, and it continues to be one of the most precise probes of weak neutral-current interactions. Copious data now exist on the production and decay of on-shell Z and W bosons, validating the Standard Model below the 1% level. Precision neutrino studies serve to verify the theory over a wide range of Q^2 values and give unique tests of the neutrino coupling in weak processes. Neutrino scattering measurements

probe the weak interaction away from the W and Z poles and are inherently sensitive to processes beyond the Standard Model, such as leptoquark and new Z′ exchange[5] or new neutrino properties[6].

2.1 NuTeV Experiment and Technique

The NC/CC ratio is the easiest to measure experimentally. For an isoscalar nucleon target composed of equal numbers of u and d quarks, the NC to CC cross section ratio for neutrinos and antineutrinos is given by the simple relationship[7] in terms of the weak mixing angle, $\sin^2\theta_W$:

$$R^{\nu(\overline{\nu})} = \frac{\sigma_{NC}^{\nu(\overline{\nu})}}{\sigma_{CC}^{\nu(\overline{\nu})}} = \frac{1}{2} - \sin^2\theta_W + \frac{5}{9}\sin^4\theta_W \ \left(1 + r^{(-1)}\right) \text{ with } r = \frac{\sigma_{CC}^{\overline{\nu}}}{\sigma_{CC}^{\nu}} \simeq 0.5.$$

The ratio of the cross section differences[8] has the advantage of in being primarily sensitive to valence quark contributions; these contributions are more insensitive to strong interaction and heavy quark corrections:

$$R^- = \frac{\sigma_{NC}^{\nu} - \sigma_{NC}^{\overline{\nu}}}{\sigma_{CC}^{\nu} - \sigma_{CC}^{\overline{\nu}}} = \frac{R^{\nu} - rR^{\overline{\nu}}}{1 - r} = \frac{1}{2} - \sin^2\theta_W.$$

In order to use these expressions for $R^{\nu(\overline{\nu})}$ and R^-, many experimental, QCD, and radiative corrections need to be applied.[9] The most notable QCD correction is related to kinematic suppression of CC charm production due to charm quark mass effects. Uncertainties in this correction hampered precision neutrino measurements previous to NuTeV [10] to a precision of $\Delta\sin^2\theta_W = 0.0041$, equivalent to a W mass measurement at the 210 MeV level. In order to minimize such uncertainties, NuTeV exploited an R^- type measurement where charm quark and other sea quark effects tend to cancel. An R^- measurement requires pure neutrino or antineutrino running, which NuTeV could accomplish with its new high-purity, high-intensity, sign-selected neutrino beam.

Accelerator-produced neutrino beams are typically made using neutrinos from pion and kaon decay, $\pi/K \rightarrow \mu + \nu_\mu$. The NuTeV sign-selected beam used 800 GeV protons from the Fermilab Tevatron hitting a BeO target. Pions and kaons produced in the target were sign-selected using dipole magnets and then focused using quadrupole magnet into a 500 meter long decay pipe. One kilometer of earth and steel shielding stopped all hadrons and ranged out the decay muons leaving only neutrinos to interact in the NuTeV neutrino detector. The number of particles at each stage starts with 10^{13} protons hitting the target every 60 seconds, producing 2×10^{12} pions and kaons in the decay

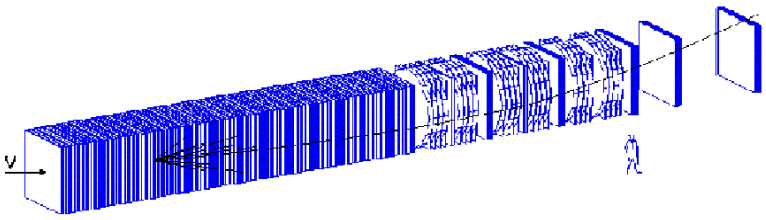

Figure 2. The NuTeV neutrino detector showing the target-calorimeter followed by the solid-iron muon spectrometer.

pipe. The decays of these mesons produce about 3×10^{10} neutrinos impinging on the NuTeV detector, which in turn give about 30 neutrino interactions in the 690 tons of the detector. The beam is very pure with a $\overline{\nu}(\nu)$ contamination of 3×10^{-4} $\left(4 \times 10^{-3}\right)$ respectively for neutrino (antineutrino) running. The sign-selected beam also minimizes electron neutrino contamination (an important background for isolating true NC events) from K decay to the ˜1.6% level.

The NuTeV neutrino detector (Fig. 2) consists of a 690 ton target calorimeter composed of four inch steel plates interspersed with liquid scintillation counters and drift chambers. The counters were used to determine the longitudinal vertex of the neutrino interaction and, through calorimetric methods, to determine the hadronic energy of the event. The drift chambers localized the transverse interaction point and tracked the muon through the target. For the NuTeV electroweak measurements, each neutrino event was characterized by the visible hadronic energy, E_{had}; the vertex position; and the event length, determined from the first and last counter with at least a minimum ionizing pulse height. The target calorimeter was followed by a toroidally magnetized iron spectrometer to measure the momentum of muons emerging from the CC neutrino interactions. The spectrometer was not used for NC/CC event separation but only to measure the energy distribution of the CC event sample so that the incident neutrino flux as a function of energy could be determined.

2.2 NuTeV Measurement and Results

Observed events were separated into NC and CC candidates statistically using the event length. The experimental quantities $R^{\nu}_{\rm exp}$ and $R^{\overline{\nu}}_{\rm exp}$ were determined

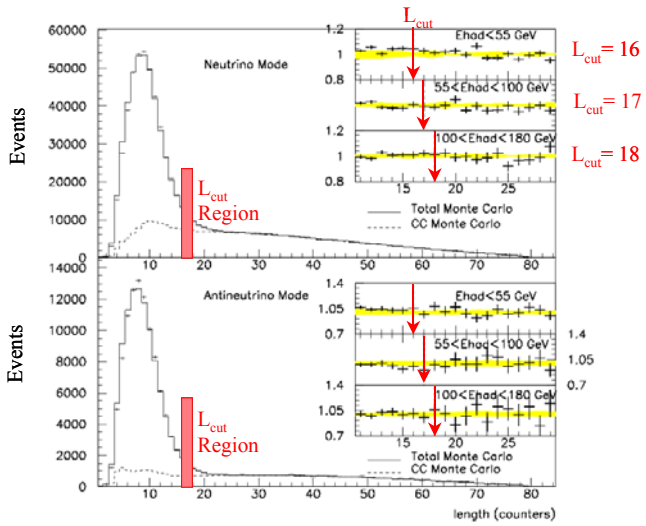

Figure 3. Comparison of ν and $\overline{\nu}$ event length distributions in data and Monte Carlo (MC). The MC prediction for CC events is shown separately. Insets show data/MC ratio comparisons in the region of the length cut with bands to indicate the 1σ systematic uncertainty in this ratio.

using a separation length cut, L_{cut}:

$$R_{\rm exp} = \frac{\text{SHORT events}}{\text{LONG events}} = \frac{L \le L_{cut}}{L > L_{cut}} = \frac{\text{NC Candidates}}{\text{CC Candidates}}$$

The value of L_{cut} was changed as a function of E_{Had} and was 16, 17, and 18 for $E_{had} < 55$, $55 < E_{had} < 100$, and $100 < E_{had} < 180$ GeV respectively. With this L_{cut} definition, the candidate numbers were

	Short (NC)	Long (CC)	$R_{\rm exp}$ =Short/Long
Neutrino	475,000	1,167,000	0.3916 ± 0.0007
Antineutrino	101,000	250,000	0.4050 ± 0.0016

The procedure[9] for using $R^{\nu}_{\rm exp}$ and $R^{\overline{\nu}}_{\rm exp}$ to extract $\sin^2\theta_W$ involves a detailed Monte Carlo simulation incorporating models of the neutrino beam, the neutrino detector, and the radiatively-corrected cross sections for the neutrino scattering processes. By using simultaneous fits of the data to the predictions for $R^{\nu}_{\rm exp}$ and $R^{\overline{\nu}}_{\rm exp}$, NuTeV effectively gains the advantage of using the R^-

technique. The largest experimental uncertainty is associated with the imperfect knowledge of the $\sim 1.7\%$ $\nu_e/\overline{\nu}_e$ background, giving an uncertainty at the $\Delta \sin^2\theta_W = 0.0039$ level. Electron neutrino events nearly always appear as short NC candidates, so understanding these events is critical. The NuTeV beamline suppresses the poorly known K^L_{e3} source and the $K^{\pm}_{e3}$ and charm decay sources are constrained by the observed high, energy ν_μ and wrong-sign events respectively. The largest model uncertainly in the extraction arises from residual dependence of charged-current charm production, giving an uncertainty of $\Delta \sin^2\theta_W = 0.0047$. The uncertainty has been greatly reduced through the effective R^- technique, which has been verified by others[11].

Using the above technique, a single-parameter fit to $R^{\nu}_{\rm exp}$ and $R^{\overline{\nu}}_{\rm exp}$ with all other parameters assumed to have their standard values (e.g., standard electroweak radiative corrections with $\rho_0 = 1$) yields

$$\begin{aligned}\sin^2\theta_W^{(on-shell)} &= 0.2277 \pm 0.0013(stat.) \pm 0.0009(syst.) \\ &\quad -0.00022 \times \left(\frac{M^2_{top} - (175\ GeV)^2}{(50\ GeV)^2}\right) \\ &\quad +0.0032 \times \ln\left(\frac{M_{Higgs}}{150\ GeV}\right).\end{aligned}$$

The extraction has been done using the on-shell scheme[12] for radiative corrections where the weak mixing angle is directly related to the physical boson masses, $\sin^2\theta_W^{(on-shell)} \equiv 1 - M^2_W/M^2_Z$. Using the central NuTeV value and the precisely known Z^0 mass gives a derived value of $M_W = 80.14 \pm 0.08$ GeV. The new NuTeV result is a factor of two more precise than the previous neutrino world average ($\sin^2\theta_W = 0.2277 \pm 0.0036$), and is dominated by statistical uncertainty. A fit to the precision electroweak data, excluding neutrino measurements, predicts a value of 0.2227 ± 0.00037, approximately 3σ from the NuTeV measurement. An alternative single-parameter fit to the ρ_0 parameter gives $\rho_0 = 0.9942 \pm 0.0013(stat.) \pm 0.0016(syst.)$ indicating that the NuTeV NC coupling is about 1% less than expected. Finally, two-parameter fits have been performed to the effective neutral-current u and d quark couplings, $g^2_{L,R} = u^2_{L,R} + d^2_{L,R}$. (These fits relax the Standard Model assumptions for electroweak corrections but do apply the QED corrections that approximately factor.) NuTeV's results are:

$$g^2_L = 0.30005 \pm 0.00137;\ g^2_R = 0.03076 \pm 0.00110.$$

2.3 Comparisons and Implications

The NuTeV results differ substantially from the Standard Model predictions [13] using other precision measurements (Fig. 4). The NuTeV fit values (not all independent) and predictions are shown in the table below.

Parameter	NuTeV Value	SM Prediction
$\sin^2\theta_W$	0.2277 ± 0.0016	0.2227 ± 0.0004
M_W	80.14 ± 0.08	80.45 ± 0.04
ρ_0	0.9942 ± 0.0021	1.0
$R^{\nu}_{\rm exp}$	0.3916 ± 0.0013	0.3950
$R^{\overline{\nu}}_{\rm exp}$	0.4050 ± 0.0027	0.4066
g_L^2	0.30005 ± 0.00137	0.3042
g_R^2	0.03076 ± 0.00110	0.0301

For the multi-parameter data, the discrepancy is in $R^{\nu}_{\rm exp}$ and the g_L^2 coupling. The global electroweak fit including NuTeV gives a $\chi^2/df = 28.2/15$ with a 1.7% probability; dropping NuTeV from the fit yields $\chi^2/df = 19.6/14$ with 14% probability. The poor χ^2 for the global fit comes from the NuTeV measurement and from the $A_{fb}^{0,b}$ asymmetry measurements. At this point, one cannot rule out the possibility of a statistical flucuation but pne should also consider alternative physics explanations.

Alternative explanations fall into two general categories: modified Standard Model effects and new physics effects. Plausible Standard Model effects that NuTeV did not explicitly account for in its analysis include nuclear shadowing, asymmetries in the nucleon strange sea, and nucleon-level isospin violation. Investigations show that none of these effects appear able to explain the full discrepancy. Nuclear shadowing should deplete the CC relative to NC processes[14] in heavy nuclei, which would move the extracted $R^{\nu/\overline{\nu}}$ to an even larger value. NuTeV dimuon measurements restrict the size and sign of an strange/anti-strange quark momentum asymmetry, again moving the $R^{\nu/\overline{\nu}}$ to larger values.[15] Isospin conservation is assumed in the NuTeV analysis with $u_p = d_n$ and $d_p = u_n$. A violation of this symmetry could effect the analysis since the u and d quark couplings are different. Recent bag model calculations[16] yield estimates that would introduce only small shifts in $\sin^2\theta_W$ at the 10^{-4} level. Future results from global parton distribution fits may eventually constrain experimentally the size of isospin violating effects.

New physics explanations of the NuTeV anomaly are highly constrained by other precision measurements. Davidson *et al.* show that the following models do not work[11]: anything generating oblique type electroweak corrections, models of anomalous neutrino couplings, an extra Z′ with generation-

Figure 4. The precision data, as compiled and fit by the LEPEWWG.[13] The global fit χ^2 is 28.8 for 15 dof.

independent $SU(2)_L$ couplings, low energy minimal supersymmetry, and $SU(2)$ singlet or doublet leptoquarks. New physics models they identify that can make a significant contribution are contact interactions, possibly mediated by vector leptoquarks at ˜1.4 TeV, and a new $U(1)$ $B-3L_\mu$ gauge symmetry containing a Z′ that decouples from the first generation leptons and mixes with the SM Z. An another example is the extended supersymmetry model with an $SO(10)$ gauge symmetry by Babu and Pati.[17] Neutrino oscillations of electron neutrinos to sterile neutrinos have been proposed by Giunti and Laveder[18] and could explain the anomaly if the oscillation probability were as large as $P(\nu_e \rightarrow \nu_s) = 0.21 \pm 0.07$ for $\Delta m^2 = 10 - 100\ eV^2$. Oscillations at this level are close to being excluded by previous data including that from NuTeV. In summary, new physics models exist that can explain

the NuTeV measurement, but the models are not simple extensions of the Standard Model.

3 Neutrino Properties: Mass and Oscillations

There is no fundamental reason why neutrinos must be massless, and since they are the SM partners of the massive charged leptons, it would be natural for neutrinos also to be massive. But it is clear that their masses are much smaller than the charged leptons, and we would like to understand the reason from a theoretical point of view. Cosmologically, massive neutrinos could play an important role in the evolution of the universe as well as in structure formation. With the universe filled with $10^9\nu/\mathrm{m}^3$, even a small mass at the level of ~ 1 eV will have significant effects. Structure formation models with hot (ν) and cold dark matter are close to having sensitivities at the 1 eV level. Current measurements can be interpreted to limit the contribution of neutrinos to the matter density of the universe between $0.003 < \Omega_\nu < 0.20$.

In the SM, only left-handed neutrinos exist and a standard Dirac mass term in the Lagrangian cannot be constructed. For this reason, models with massive neutrinos require extensions to the SM. These extensions can give neutrino masses through grand unified theories with heavy right-handed neutrinos, through modified Higgs sectors with additional possibilities for mass terms, and through extra dimension models where right-handed neutrinos can propagate into the bulk. In many of these extended models, there exists at least one electroweak isosinglet or *sterile* ν. These sterile neutrinos could be the right-handed partners of the SM left-handed ν and are "sterile" with respect to interactions with the standard W and Z bosons.

An interesting possibility is the class of grand unified theories that contain both Dirac and Majorana mass terms. For Dirac neutrinos the neutrino and antineutrino are distinct particles. Lepton number is conserved and neutrinos couple with the W to produce a negatively charged lepton. In the Lagrangian, the Dirac mass term would be $m_D(\overline{\nu}_L\nu_R+\overline{\nu}_R\nu_L)$. On the other hand, a Majorana neutrino would have the property that the neutrino and antineutrino are the same particle only differing by their handedness. Neutrinos are the left-handed component that produces negative charged leptons and antineutrinos are the right-handed component giving positive charged leptons. Obviously, if Majorana neutrinos exist, then lepton number is not conserved since a neutrino can be changed to an antineutrino by flipping the spin. The Majorana mass term becomes $m_M^L\left(\overline{\nu}_L(\nu_L)^c + (\overline{\nu}_L)^c\,\nu_L\right)+m_M^R\left(\overline{\nu}_R(\nu_R)^c + (\overline{\nu}_R)^c\,\nu_R\right)$. In models with both Dirac and Majorana mass terms, the combined mass matrix needs to be diagonalized leading to the *"see-saw"* mechanism for generating

a small neutrino mass. The total Lagrangian is given by

$$\mathcal{L}_{mass} = -\frac{1}{2}\left(\overline{\nu}_L \ (\overline{\nu}_R)^c\right)\mathcal{M}\begin{pmatrix}(\nu_L)^c\\ \nu_R\end{pmatrix} \text{ with } \mathcal{M} = \begin{pmatrix}m_M^L & m_D\\ m_D & m_M^R\end{pmatrix}$$

One assumes that the right-handed Majorana mass m_M^R is very large, the left-handed mass m_M^L is very small, and the Dirac mass m_D is similar to standard quark or charged lepton masses. The hierarchy then becomes $m_M^R = M \gg m_D \gg m_M^L \approx 0$. Diagonalizing this mass matrix leads to two eigenstates, a large one m_N associated with a isosinglet sterile neutrino and a small one associated with the Standard Model light neutrinos.

$$m_N \approx M \text{ and } m_\nu \approx \frac{m_D^2}{M}$$

4 Direct Neutrino Mass Experiments

A variety of techniques have been used to search directly for neutrino mass effects in the weak decay of particles and nuclei. The most sensitive searches have been associated with electron neutrinos. Here, the tritium decay process

$$^3H \rightarrow ^3 He + e^- + \overline{\nu}_e$$

is investigated near the kinematic endpoint of the outgoing electron spectrum. A finite neutrino mass would distort the spectrum near the endpoint as

$$dN(E) = \mathcal{K}|M|^2 F(Z,E,E) p_e E (E_0 - E)\left\{(E_0 - E)^2 - m_\nu^2\right\} dE$$

The sensitivity is related to the number of decays probed within a few eV of the endpoint. About 2×10^{-13} happen within the last 1 eV region, making the measurement very challenging. No indication of neutrino mass has been seen, and the current best limit is from the Mainz group constraining $m_{\nu_e} < 2.2$ eV at 95% CL. A new KATRIN collaboration [19] of previous experimental groups has been formed to perform a next-generation experiment scaling up the size of previous experiments by an order of magnitude with a much more intense tritium source. The new experiment should have sensitivities down to 0.35 eV masses.

Muon neutrino masses can be probed by precision studies of the muon decay spectrum from pion decays.

$$\pi \rightarrow \mu + \nu$$

Experiments have used both π decay at rest, where the pion mass dominates the uncertainty; and π decay in flight, where the resolution on measuring $p_\pi - p_\mu$ limits the sensitivity. The best limit at present is from a decay at

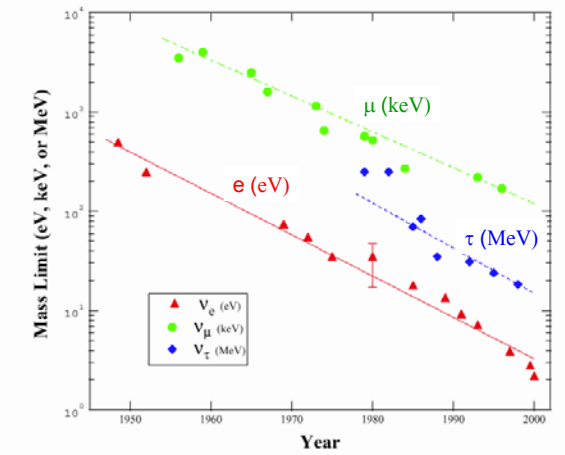

Figure 5.

rest measurement[20] giving a limit of $m_{\nu_\mu} < 170$ keV at 95% CL. There are some recent ideas to improve this bound by using the g-2 experimental setup at Brookhaven where sensitivities down to $m_{\nu_\mu} < 8$ keV may be possible.

High multiplicity tau lepton decays provide a laboratory for direct tau neutrino mass investigations. Tau lepton decays are measured near the edge of the allowed kinematic range for tau decays in the processes

$$\tau^- \rightarrow 2\pi^-\pi^+\nu_\tau \text{ and}$$
$$\tau^- \rightarrow 3\pi^-2\pi^+(\pi^0)\nu_\tau$$

Fits are made to the scaled visible energy and scaled invariant mass looking for an excess of events near the kinematic boundary. The current best limit [21] is from the Aleph experiment at LEP giving a limit of $m_{\nu_\mu} < 18.2$ MeV at 95% CL. The history of direct neutrino mass measurements is given in Figure and shows impressive progress over the years with a Moore's power law dependence.

Double beta decay studies are a unique method to probe for massive Majorana neutrinos. In certain nuclei, single β (electron) decay is energetically not allowed (^{136}Xe $\rightarrow$ ^{136}Ba,^{76}Ge $\rightarrow$ ^{76}Se, etc.) For these nuclei, double β-decay transitions are possible with long lifetimes due to the double weak transition $\propto G_F^4$. In these transitions, the atomic number is increased by two units, and two electrons and two neutrinos are emitted. The undetected

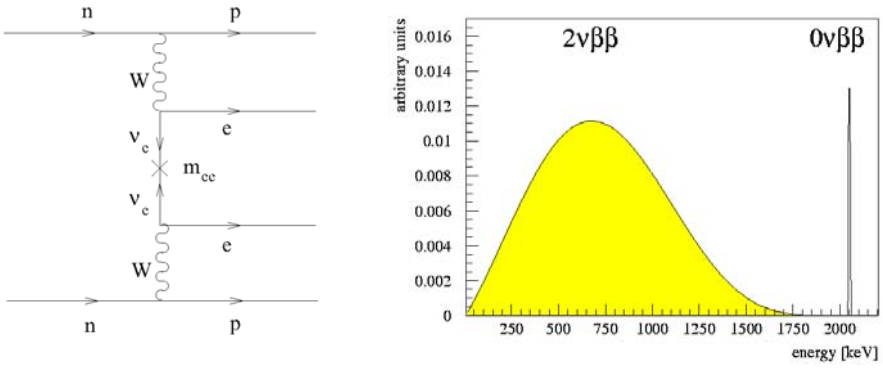

Figure 6.

neutrinos lead to broad visible energy spectrum for the two electrons:

$$(Z, A) \rightarrow (Z + 2, A) + (e^- e^- \overline{\nu}_e \overline{\nu}_e) \quad 2\nu\beta\beta \text{ decay.}$$

If neutrinos are Majorana particles, then one can also have the 0ν transitions where the sum of the visible electron energies is monoenergetic:

$$(Z, A) \rightarrow (Z + 2, A) + (e^- e^-) \quad 0\nu\beta\beta \text{ decay.}$$

Experimentally, one looks for 0ν signal in the visible energy spectrum beyond the 2ν endpoint energy. The rate of $0\nu\beta\beta$ decays is proportional to $(m_\nu/m_e)^2$ and can, thus, be used to probe for a finite neutrino mass.

The current best limit comes from the Heidelberg-Moscow experiment[22] using 24 kg-yrs of ^{76}Ge data leading to a lifetime limit of 5.7×10^{25} years and a mass limit of $m_{\nu_e} < 0.2$ eV at 90% CL. Proposed future experiments include: a new ^{76}Ge experiment (GENIUS) with several tons of detector and a sensitivity to ∼few $\times 10^{-3}$ eV, and a new $^{136}\text{Xe} \rightarrow {}^{136}\text{Ba}$ experiment (EXO) using a time projection chamber technique to track both the $e^- e^-$ and Ba atom and having a sensitivity at the ∼0.01 eV level.

Supernova explosions also offer a testing ground for neutrino mass. In a supernova explosion over 99% of the energy is carried away by neutrinos; these neutrinos escape the exploding star before the photons. The rate of escape for ν_e's is different from ν_μ's and ν_τ's, due to the extra ν_e CC interactions with electrons. Neutrino mass limits can be obtained by the spread in the propagation time; there will be a spread in arrival times for different energies if $m_\nu \neq 0$ with $t_{obs} - t_{emit} = t_0 \left(1 + m^2/2E^2\right)$. For SN1987a, the neutrinos

were detected in the Kamiokande and IMB detectors with about a spread of $\sim$13 seconds after traveling 180,000 light years, with energies that differed by up to a factor of three. The neutrinos arrived about 18 hours before the light was seen. Assuming that the emission time happened over a 4 second interval, the data has been used to set a limit on the neutrino mass of $m_\nu <\sim 30$ eV. For the future, a network (SNEWS − The Supernova Early Warning System) of the world's ν observatories has been set up to provide an early coincidence signal to trigger detection by experiments of any detectable supernova.

5 Neutrino Oscillations

As we have seen, it is difficult to probe small values of neutrino mass especially for the ν_μ and ν_τ using direct measurement techniques. Obtaining sensitivity to lower mass values requires a new method, neutrino oscillations. Neutrino oscillations are a quantum mechanical process where one type of neutrino changes into another type of neutrino due to different mass eigenstate combinations. For the phenomenon to take place, there needs to be mass eigenstates of different masses, and the flavor types need to be different combinations of these mass eigenstates. As an example consider the two flavor mixing of the ν_e and ν_μ neutrinos in terms of neutrino mass eigenstates ν_1 , ν_2 ,and the mixing angle θ:

$$\begin{pmatrix} \nu_e \\ \nu_\mu \end{pmatrix} = \begin{pmatrix} \cos\theta & \sin\theta \\ -\sin\theta & \cos\theta \end{pmatrix} \begin{pmatrix} \nu_1 \\ \nu_2 \end{pmatrix}.$$

If we assume at $t = 0$, the neutrino is created as a muon neutrino ν_μ, then

$$|\psi(0)\rangle = |\nu_\mu(0)\rangle = -\sin\theta|\nu_1\rangle + \cos\theta|\nu_2\rangle.$$

At a later time t, the two mass states will have propagated with different phases leading to a ν_e/ν_μ mixture:

$$\begin{aligned} |\psi(t)\rangle &= -\sin\theta\ e^{-iE_1 t}\ |\nu_1\rangle + \cos\theta\ e^{-iE_2 t}\ |\nu_2\rangle \\ &= \left(\cos^2\theta\ e^{-iE_1 t}\ + \sin^2\theta\ e^{-iE_2 t}\right)|\nu_e\rangle \\ &\quad + \sin\theta\cos\theta\left(\ e^{-iE_2 t} - \ e^{-iE_1 t}\right)|\nu_\mu\rangle. \end{aligned}$$

The oscillation probability for $\nu_\mu \to \nu_e$ is then given by

$$P_{osc} = |\langle\nu_e|\psi(t)\rangle|^2 = \frac{1}{2}\sin^2 2\theta\left[1 - \cos(E_2 - E_1 t)\right].$$

For small masses, $E_1 = p + m_1^2/2p$ and $E_2 = p + m_2^2/2p$ and $(t/p) = L/E$, yielding:

$$\begin{aligned} P_{osc} &= \frac{1}{2}\sin^2 2\theta \left(1 - \cos\left(\frac{\left(m_2^2 - m_1^2\right)L}{E}\right)\right) \\ &= \sin^2 2\theta \sin^2\left(1.27\ \Delta m^2\left(eV^2\right)\frac{L(\mathrm{m})}{E(\mathrm{GeV})}\right). \end{aligned}$$

where the factor 1.27 in the last formula depends on the units, after substituting for the use of $\hbar = c = 1$.

Of course, there are three neutrinos and may even be more if there are sterile ones. The three generation mixing formalism uses a matrix similar to the quark CKM matrix called the MNS (Maki-Nakagawa-Sakata) matrix:

$$\begin{pmatrix} \nu_e \\ \nu_\mu \\ \nu_\tau \end{pmatrix} = \begin{pmatrix} c_{12}c_{13} & s_{12}c_{13} & s_{13}e^{-\delta} \\ -s_{12}c_{23} - c_{12}s_{23}s_{13} & c_{12}c_{23} - s_{12}s_{23}s_{13}e^{i\delta} & s_{23}c_{13} \\ s_{12}s_{23} - c_{12}c_{23}s_{13}e^{i\delta} & -c_{12}s_{23} - s_{12}c_{23}s_{13}e^{i\delta} & c_{23}c_{13} \end{pmatrix} \begin{pmatrix} \nu_1 \\ \nu_2 \\ \nu_3 \end{pmatrix},$$

where c and s refer to the sines and cosines of the three mixing angles, θ_{12}, θ_{23},and θ_{13}; and δ is a complex phase associated with CP violation. With three generations, there are three Δm_{12}^2, Δm_{23}^2, and Δm_{13}^2, but only two are independent.

It is not usually appreciated that for each Δm_{ij}^2 value, there can be oscillations among all the neutrino flavors, but with different combinations of mixing angles. For example, oscillations corresponding to the Δm_{23}^2 term include:

$$\begin{aligned} P\left(\nu_\mu \to \nu_\tau\right) &= \cos^4\theta_{13}\sin^2 2\theta_{23}\sin^2\left(1.27\Delta m_{23}^2 L/E\right) \\ P\left(\nu_\mu \to \nu_e\right) &= \sin^2\theta_{23}\sin^2 2\theta_{13}\sin^2\left(1.27\Delta m_{23}^2 L/E\right) \\ P\left(\nu_e \to \nu_\mu\right) &= \cos^2\theta_{23}\sin^2 2\theta_{13}\sin^2\left(1.27\Delta m_{23}^2 L/E\right) \end{aligned}$$

Observation of CP violation in neutrino oscillations has been put forward as a prime future goal for the field, since it may give us a key to the source of neutrino mass and may also be important for understanding the baryon versus anti-baryon asymmetry in the universe. But seeing CP violating effects in neutrino oscillations is going to be very difficult. The reason is that one can only observe these effects through an experiment that is sensitive to oscillations involving at least three different types of neutrinos. One possibility is comparing the probability for $\nu_\mu \to \nu_e$ versus $\overline{\nu}_\mu \to \overline{\nu}_e$ oscillations.

$$P\left(\nu_\mu \to \nu_e\right) - P\left(\overline{\nu}_\mu \to \overline{\nu}_e\right) = 4\,\mathrm{Im}\left(U_{\mu 1}U_{e1}^* U_{\mu 3}^* U_{e3}\right)\left(s_{12} + s_{23} + s_{31}\right)$$

where U_{ij} are the elements of the MNS matrix ($4\,\mathrm{Im}\left(U_{\mu 1}U_{e1}^{*}U_{\mu 3}^{*}U_{e3}\right) = 16c_{12}c_{13}^{2}c_{23}s_{12}s_{13}s_{23}\left(\sin\delta\right)$), and $s_{ij} = \sin\left(\Delta m_{ij}^{2}L/2E\right)$. (Note: in this formula the s_{ij} terms are not squared but add linearly.) To have sensitivity to this CP violating difference, the combination of mixing angles must be finite and all the terms (s_{12}, s_{23}, s_{31}) must not be small (or effectively one would have two component oscillations). For example, if $s_{12} \approx 0$ then $s_{23} \approx -s_{31}$ and the sum $s_{12} + s_{23} + s_{31} \approx 0$. This means that an experiment must be sensitive to the lowest Δm^2 value, which currently would be that associated with solar neutrino oscillations.

5.1 Neutrino Oscillation Phenomenology

There are two types of neutrino oscillation experiments, appearance and disappearance searches. For an appearance search, an experiment looks for the anomalous appearance of ν_e or ν_τ events in a relatively pure ν_μ beam and studies this as a function of distance, L, and energy, E. This type of experiment is mainly sensitive to uncertainties in background sources of appearance neutrinos. In a disappearance experiment, one looks for a change in the beam ν flux as a function of L and E. This type of experiment relies on knowing accurately the neutrino flux and interaction cross sections. The range of values for the parameters, Δm^2 and $\sin^2 2\theta$, sets the demands on the search experiment. The mixing angle $\sin^2 2\theta$ sets the size of oscillation effects and thus the needed statistical sample. The Δm^2 value sets the distance to energy ratio needed for the neutrinos to oscillate with an oscillation length given by $L_{osc} = \pi E/\left(1.27\Delta m^2\right)$.

Results from oscillation experiments are typically displayed on a two dimensional plot of Δm^2 versus $\sin^2 2\theta$ (Fig. 7) assuming an effective two component mixing formula. If an experiment sees an oscillation signal with a probability given by $P_{osc} = P_{signal} + \delta P_{signal}$, then, within some confidence level, a region in the (Δm^2, $\sin^2 2\theta$) plane is allowed. If, on the other hand, an experiment sees no signal and limits the probability of a specific oscillation channel to be $P_{osc} < P$ at 90% CL, then an excluded region is displayed in the (Δm^2, $\sin^2 2\theta$) plane.

The current experimental situation is displayed in Fig. 8. This plot shows three signal regions associated with solar, atmospheric, and LSND oscillation experiments. There have also been many negative searches that exclude many parts of the plot away from these signals and the region at higher Δm^2.

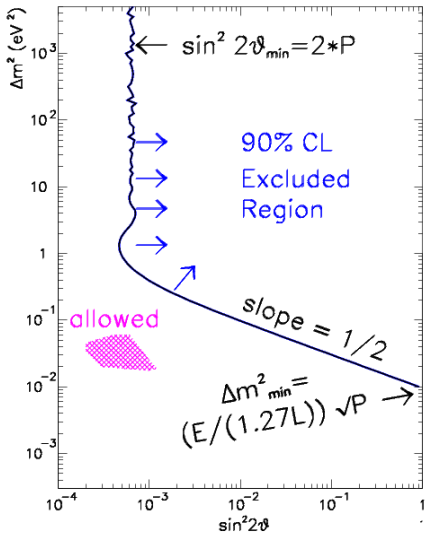

Figure 7. Generic oscillation plot showing an allowed region for a positive signal and an excluded region from an experiment that limits the oscillation to be less than P at 90% CL.

6 Solar Neutrino Oscillation Experiments

Solar neutrino studies offer a unique tool to probe for neutrino oscillations at very small Δm^2. The neutrinos are produced in the nuclear processes in the sun, and give neutrino energy ranging from the 0.1 MeV up to 10 MeV. Combining this energy with the large sun-to-earth distance (1.5×10^{11} m) gives sensitivity to Δm^2 values below 10^{-10} eV^2. Since the early 1970's, there have been indications that the solar neutrino flux at the earth is much less than expected, and over the years mounting evidence has shown that the deficit is most likely due to neutrino oscillations. The recent data from the SNO experiment have shown that the deficit of electron neutrinos is correlated with an appearance of muon and tau neutrinos. The goals of the experiments are now turning to accurately determining the oscillation parameters, Δm^2 and $\sin^2 2\theta$.

The Standard Solar Model (SSM) is used to predict the neutrino flux at the earth and incorporates many experimental and theoretical inputs. The SSM uses a stellar evolution model with hydrodynamic equilibrium between pressure and gravity, energy transport by radiation and convection, and en-

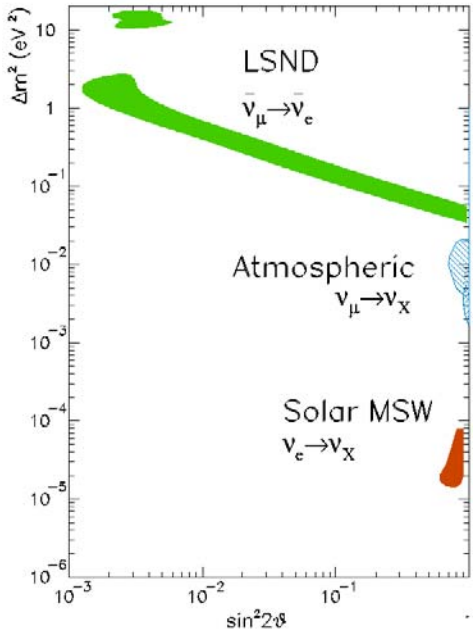

Figure 8. Oscillation signals from current experimental results.

ergy production by nuclear reactions. The model is constrained by the physical measurements of the sun including seismic, temperature, and diffusion data. The output of the SSM is the solar temperature and density as a function of radius, and the neutrino flux.

As seen in Fig. 9, many of the solar nuclear processes lead to neutrinos. The energy spectrum is shown in Fig. 10 along with the regions covered by the various experimental techniques. From the solar luminosity, the main pp neutrino flux is known to 1%; the flux from other processes such as the ^{7}Be and ^{8}B neutrinos have a 10% to 20% uncertainty.

There are two types of solar neutrino experiments, the chemical extraction experiments (Homestake, Sage, and Gallex) and the scattering experiments (Super-Kamiokande and SNO). The Homestake experiment in the Homestake mine in Lead, South Dakota detects solar neutrinos through the process $\nu_e + {}^{37}\mathrm{Cl} \rightarrow {}^{37}\mathrm{Ar} + e^-$; as seen in Fig. 10, this experiment is sensitive to solar neutrinos above 0.9 MeV. The gallium experiments, Sage and Gallex, use the

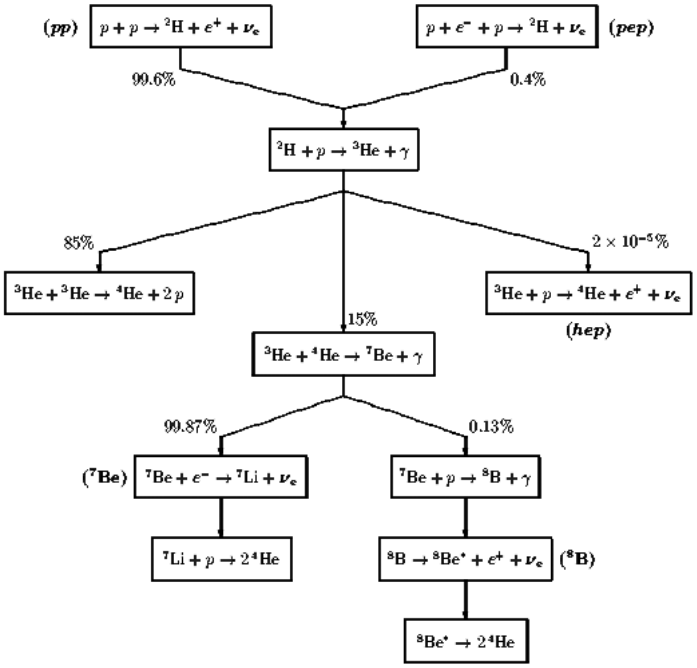

Figure 9. The solar processes with relative percentage probabilities for the various chains.

process $\nu_e + {}^{37}\mathrm{Ga} \rightarrow {}^{37}\mathrm{Ge} + e^-$, which has a much lower threshold allowing the experiment to detect the primary pp neutrinos with energies down to 0.2 MeV.

The Super-K experiment uses the elastic scattering process, $\nu + e^- \rightarrow \nu + e^-$, in a 22.5 kton water detector to measure the solar flux above the few MeV region. This process has good directional information and shows a clear angular peak pointing toward for the detected solar events. The Sudbury Neutrino Observatory (SNO) uses 1 kton of heavy water as a target. For heavy water, deuterium breakup processes are also observable, which increases the rate and gives the experiment sensitivity to NC scattering by any flavor

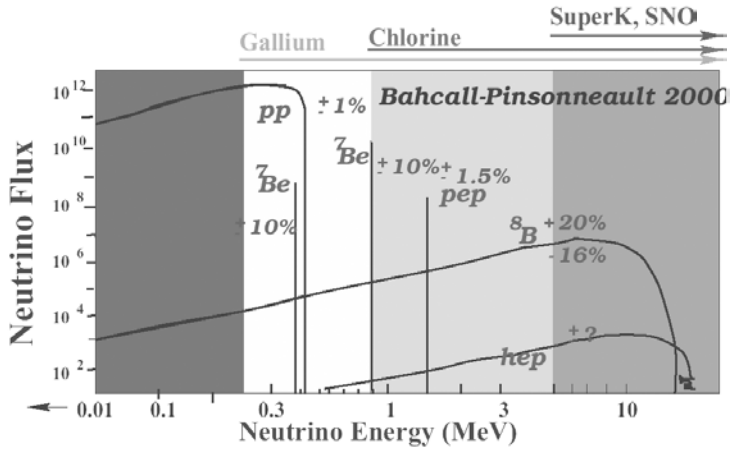

Figure 10. The energy spectrum for the relative solar neutrino flux from the various processes in the sun. Also shown is the energy range covered by the various experimental techniques.

neutrino:

$$\begin{aligned} \nu_e + d \rightarrow p + p + e^- \quad & \text{SNO CC} \\ \nu_x + d \rightarrow p + n + \nu_x \quad & \text{SNO NC} \\ \nu_x + e^- \rightarrow \nu_x + e^- \quad & \text{Super-K and SNO.} \end{aligned}$$

In addition, the cross section for scattering from neutrons is much larger than scattering from electrons, giving the SNO experiment an 8 event/day solar rate for 1 kton of heavy water versus the 25 event/day rate in the Super-K 22 kton light water detector. As will be shown later, the comparison of the SNO NC and CC processes along with the elastic scattering data allows information to be obtained on the neutrino flux as a function of flavor.

All solar neutrino experiments see a deficit in the observed versus the predicted rate.

Experiment	Reaction	Observed/Predicted Rate
Homestake (USA)	$\nu_e + {}^{37}Cl \rightarrow {}^{37}Ar + e^-$	0.34 ± 0.03
SAGE (Russia)	$\nu_e + {}^{37}Ga \rightarrow {}^{37}Ge + e^-$	0.59 ± 0.06
GALLEX (Italy)	$\nu_e + {}^{37}Ga \rightarrow {}^{37}Ge + e^-$	0.58 ± 0.05
Super-K (Japan)	$\nu_x + e^- \rightarrow \nu_x + e^-$	0.46 ± 0.02
SNO (Canada)	$\nu_e + d \rightarrow p + p + e^-$	0.35 ± 0.03

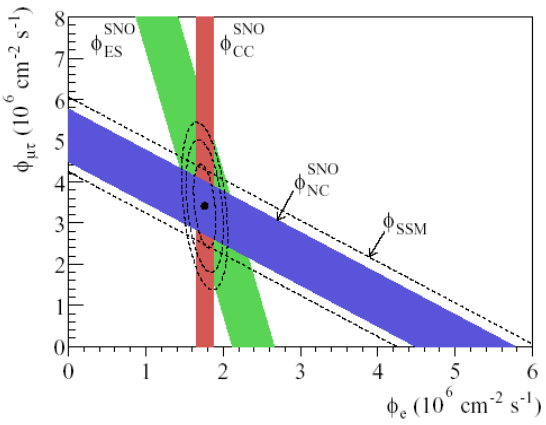

Figure 11. Flux of ^{8}B solar neutrinos which are μ or τ flavor versus the flux of electron neutrinos deduced from the three different neutrino reactions in SNO. The diagonal bands show the total ^{8}B flux as predicted by the SSM (dashed line) and that measured with the NC reaction in SNO (solid band).

Recently, the SNO collaboration has presented new results[23] on their solar NC measurements, $\nu_x + d \rightarrow p + n + \nu_x$. The process is sensitive to all active neutrino flavors including ν_e, ν_μ, and ν_τ, and therefore measures the total active neutrino flux coming from the sun. The NC measurement gives a total flux of $5.09 \pm 0.64 \times 10^6$ cm^{-2}s^{-1}, and the CC measurement gives a ν_e flux of $1.76 \pm 0.10 \times 10^6$ cm^{-2}s^{-1}. Comparing this to the SSM prediction for the ν_e flux of $5.05 \pm 1.00 \times 10^6$ cm^{-2}s^{-1} shows good agreement in the total rates but a clear indication for oscillations of electron neutrinos to other active flavors. In addition, the agreement of the total rates constrains the amount of oscillations there could be to sterile neutrinos.

In order to interpret the solar results in terms of neutrino oscillations, oscillation model fits are done to the various experimental results including experimental, theoretical, and solar model uncertainties. Matter effects in the sun and earth can be important and need to be included. (These are commonly referred to as MSW effects for the authors Mikheyev, Smirnov, and Wolfenstein who first proposed them.) These effects come about because the propagating mass eigenstates are mixtures of flavor eigenstates, which have different interaction cross sections with the electrons in the sun and earth. The cross section differences arise from the fact that electron neutrinos interact

with electrons both through the NC and CC but muon and tau neutrinos only through NC processes. If N is the electron density then the oscillation probability equation is modified to be

$$P\left(\nu_e \rightarrow \nu_\mu\right) = \left(\sin^2 2\theta / W^2\right) \sin^2\left(1.27 W \Delta m^2 L/E\right)$$
$$\text{where } W^2 = \sin^2 2\theta + \left(\sqrt{2} G_F N (2E/\Delta m^2) - \cos 2\theta\right)^2$$

This formula has a resonance with $\sin^2 2\theta_{eff} = 1$ when $\cos 2\theta = \sqrt{2} G_F N (2E/\Delta m^2)$. Matter effects occurring in the sun can give large mixings even for small $\sin^2 2\theta$ and matter effects in the earth can introduce a day-night or zenith angle effect in the observed rates. Analyses include all of these effects in constraining allowed regions. The recent SNO day-night effects paper[24] shows the current allowed regions as shown in the Fig. 12. For the past several years, there have three region in $(\Delta m^2, \sin^2 2\theta)$ plane that were allowed; the large mixing angle (LMA), small mixing angle (SMA), and LOW solutions. The new SNO paper shows that only the LMA solution now remains.

The Kamland experiment is currently running, and will test the LMA solar neutrino oscillation hypothesis with terrestrial neutrinos from nuclear reactors. The detector consists of 1000 m^3 of liquid scintillator observed by 2000 17-in phototubes in a cavern of the Kamioka mine in Japan. Anti-electron neutrinos from reactors in Japan impinge on the detector with an average distance of 170 km, and are detected for $E_\nu > 1.8$ MeV. Another 300 ton liquid scintillation experiment, Borexino, with 2200 8-in phototubes will come online shortly and primarily examine the solar neutrinos from ^{7}Be processes in the sun. A detection rate of 55 events/day is expected. The combination of these new measurements and continued data from SNO should allow, over the next several years, precise determinations of the mixing parameters for oscillations to active and possibly sterile neutrinos.

7 Atmospheric Neutrino Oscillation Experiments

Neutrinos are produced in the atmosphere from the interactions of cosmic-ray protons and nuclei with atmospheric gas molecules. These interactions produce hadronic showers with pion, kaons, and muons that can decay into neutrinos. The flux is modeled using measured cosmic-ray fluxes, and accelerator cross section measurements.[25] Geomagnetic effects are important and there is some disagreement of these calculated fluxes with atmospheric muon measurements at the 20% level.

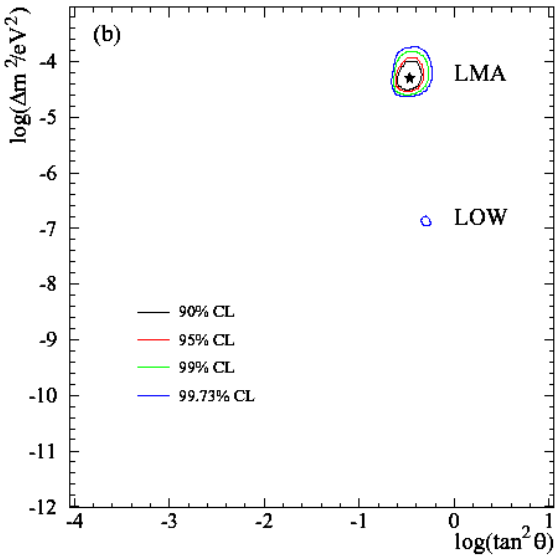

Figure 12. Allowed regions of the MSW plane determined by a χ^2 fit to the SNO day and night energy spectra and additional experimental and solar model data. The star indicates the best fit.

The energies of the atmospheric neutrinos are in the range of 100 to about 2000 MeV (Fig. 13) and therefore can be detected using interactions on protons and neutrons. The most precise measurements have come from the Super-K water Cerenkov detector where events can be classified by their Cerenkov ring configurations. Single "fuzzy" rings are electrons, sharp and filled in rings correspond to muons, and multiple rings correspond to NC and CC single pion production. Sampling calorimeter experiments can also separate event types due to their shower and penetration characteristics, as was done in the NuTeV experiment. Examples of this type of experiment include the Soudan II and future Minos experiment in the Soudan mine in Minnesota.

Several experiments have observed deficits of ν_μ events in their atmospheric data samples. The assumption is that this is due to $\nu_\mu \rightarrow \nu_\tau$ or $\nu_\mu \rightarrow \nu_{sterile}$ oscillations. The zenith or azimuthal dependence of the measured atmospheric neutrino rate in the Super-K detector has provided the most compelling evidence to date that neutrino oscillations have been ob-

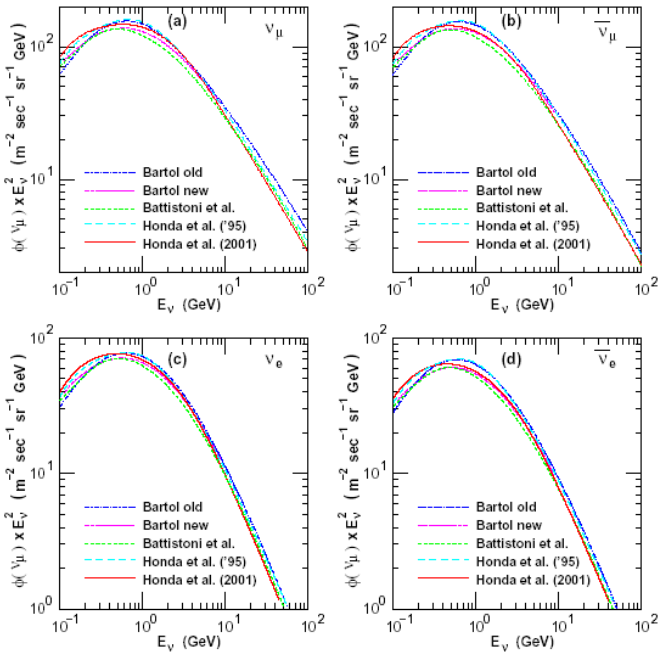

Figure 13. Comparisons of neutrino flux calculations for the location of the Super-K detector averaged over all directions. (From Ref. 25)

served. The distance from the atmospheric source for events coming from overhead ($\cos\theta_{zenith} = 1.0$) is about 15 km versus the distance for events originating on the other side of the earth ($\cos\theta_{zenith} = -1.0$) of 13,000 km. This change in distance with azimuth and the spectrum of energies from the atmospheric source provides an perfect laboratory for investigating oscillations.

The results from the Super-K experiment for 1290 days of running is shown for three energy regions in Fig. 14. These data are compared to a simulation without oscillations and with oscillations for the best fit values of $\sin^2 2\theta = 1.0$ and $\Delta m^2 = 2.4 \times 10^{-3}$ eV^2. In all three energy regions, the e-like events agree very well with the expectation with or without oscillations. On the other hand, the μ-like events show a clear deficit, which changes with zenith angle and agrees well with the oscillation hypothesis. The fact that in Fig. 14 the data agree with expectation for $\cos\theta_{zenith} = 1.0$ and shows an

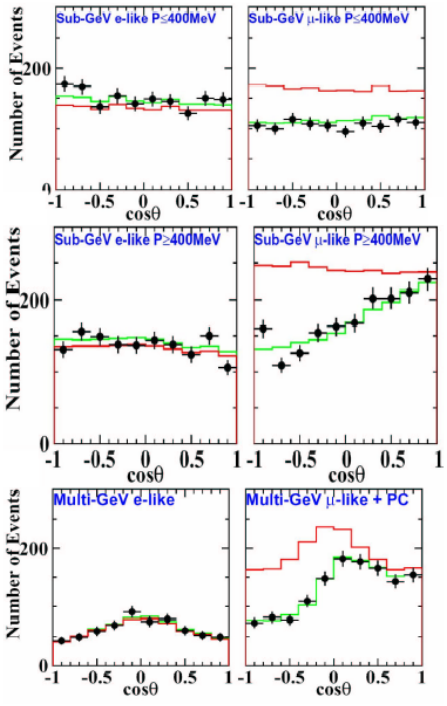

Figure 14. Zenith angle distribution of Super-K 1289 days fully contained and partially contained samples. Dots, green line, red line correspond to data, MC with no oscillations, and MC with best fit oscillation parameters, respectively.

obvious deficit at $\cos\theta_{zenith} = -1.0$ is clear evidence that the measured flux is changing with distance. The best fit values give a χ^2 of 132.4 for 137 degrees of freedom, indicating that oscillations explain the data distributions well.

The CHOOZ, Bugey, and Palo Verde reactor experiments have searched for $\overline{\nu}_e \rightarrow \overline{\nu}_\mu$ oscillations in antineutrino beams from various reactors. The mean energy of reactor antineutrinos is 3 MeV and the typical distances to the detectors are about 1 km, giving sensitivity down to $\Delta m^2 >\sim 10^{-3}$ eV^2. The CHOOZ experiment[26] has the best sensitivity in the Super-K region and, at $\Delta m^2 \approx 2 \times 10^{-3}$eV^2, limits $\sin^2 2\theta < 0.18$ at the 95% CL.

Super-K has also placed restrictions on oscillations to sterile neutrinos. [27] Three Super-K data sets are used in this study: a multi, e-like ring sample, which is enriched in NC π^0 events, expected to be be bigger for ν_τ interactions

versus $\nu_{sterile}$ interactions since the sterile neutrinos do not interact; a partially contained sample mainly composed of CC events with a mean energy of 10 GeV; and an upward through-going muon sample from CC ν_μ interactions in the matter below the Super-K detector. These last two samples are depleted near $\cos\theta_{zenith} = -1.0$ for sterile versus tau neutrinos due to matter effects with the quarks in earth, since sterile neutrinos have no NC interactions. Fits to the $\nu_\mu \to \nu_\tau$ versus $\nu_\mu \to \nu_{sterile}$ hypotheses strongly favor oscillations to tau neutrinos. Quantitatively, a 100% $\nu_\mu \to \nu_{sterile}$ hypothesis is ruled out at the 99% CL and the allowed oscillation fraction to sterile neutrinos is limited to be $< 25\%$ at 90% CL.

7.1 Long-Baseline Oscillation Experiments

Long-baseline oscillation experiments can be used to check the atmospheric results with better control of systematics, using a well-understood accelerator-produced neutrino beam. They also hold the promise of doing more detailed quantitative measurements of the oscillation parameters, and seeing directly the oscillatory behavior in energy and distance expected from oscillations versus other explanations. With high statistics and good control of systematics, these experiments can also address flavor issues: checking the existence of any $\nu_\mu \to \nu_{sterile}$ component; directly observeing ν_τ events; and looking for the sub-dominant $\nu_\mu \to \nu_e$ oscillation at the atmospheric Δm^2. With accelerator-produced neutrino beams in the few GeV energy range, the distance to a far detector must be a few hundred to a thousand km. In order to control systematics, a near detector monitoring the beam before any oscillations can take place is also an advantage.

Using the 12 GeV KEK proton synchrotron in Japan, the K2K experiment has set up a low energy neutrino beam, $\langle E_\nu \rangle = 1.4$ GeV, directed towards the Super-K detector 250 km away. The experiment also has several near detectors at a 100 m distance for monitoring the beam and for use in comparing to the rates in Super-K detector. With about half of their expected data, the experiment has seen a significant deficit of interactions in Super-K relative to the near detectors[28], observing 56 events with an expectation of 80.6 ± 8.0 events with no oscillations and 52.0 events for $\Delta m^2 = 3 \times 10^{-3}\mathrm{eV}^2$. The deficit is mainly in the region with energy below 1 GeV , is consistent with oscillations with $\Delta m^2 \approx few \times 10^{-3}\mathrm{eV}^2$, and rules out the no oscillation hypothesis at 97% CL.

This type of long baseline experiment will be continued in the future with the MINOS experiment[29]. MINOS will have a 5.4 kton detector located in the Soudan mine in northern Minnesota. A neutrino beam (NuMI - Neutri-

nos from the Main Injector) using 120 GeV protons from the Fermilab Main Injector is produced using an 800 m long decay pipe excavated in the rock below the Fermilab site and pointing down at a angle of 3.3 degrees towards Minnesota. There is also a 1 kton near detector for beam monitoring and comparison. The far (and near) detector are composed of 8 m diameter, 1 inch thick steel plates interspersed with solid scintillator planes composed of 4 cm wide long strips. The detector is 31 m long, composed of 486 layers, and magnetized with a toroidal magnetic field averaging 1.5 Tesla. The horn focusing system for the neutrino beam is flexible and can provide beams with mean energies between about 3 and 20 GeV.

MINOS is optimally set up to investigate oscillations in the atmospheric Δm^2 region. The main technique would be a disappearance measurement comparing the observed ν_μ CC rate with that derived from the near detector. With a low energy beam configuration, the experiment expects to see $\sim$700 CC events/yr in the far detector, giving sensitivity to $\Delta m^2 > 10^{-3}$ eV^2 and measurement capabilities for the oscillation parameters Δm^2 to the 10-20% level and $\sin^2 2\theta$ to 0.10. With this sample, the MINOS experiment will completely cover the Super-K atmospheric allowed region to 3.5σ. In addition, MINOS can search for a $\nu_\mu \rightarrow \nu_{sterile}$ component by measuring the CC/NC rate in the near and far detector. For $\nu_\mu \rightarrow \nu_\tau$, the CC production of τ's will look like NC events 80% of the time so the CC/NC ratio will go down relative to no oscillations. On the other hand, for $\nu_\mu \rightarrow \nu_{sterile}$ oscillations, both the CC and NC will be reduced by the same factor keeping the ratio constant.

Recently, it has been proposed to put another MINOS-prime detector at an off-axis position relative to the NuMI beamline[33]. Due to the kinematics of π-decay, the energy spectrum of the beam will be fairly mono-energetic for an angle of about 15 mr. Such a beam could allow the search for $\nu_\mu \rightarrow \nu_e$ oscillations at the atmospheric Δm^2 since the intrinsic ν_e's in the beam and the NC π^0 production from high energy ν_μ events would be significantly reduced. A 20 kton detector in this off-axis configuration could be sensitive at the 3σ level to $\nu_\mu \rightarrow \nu_e$ oscillations with $\sin^2 2\theta_{13} \approx 0.02$, which is about $\times 10$ better than the CHOOZ limit.

CERN is also planning a long-baseline program (CNGS $-$ CERN to Gran Sasso) based on two appearance experiments, OPERA and ICARUS. The experiments are to be housed in the Gran Sasso Laboratory, which is located 750 km from CERN. The neutrino beam will be produced using 400 GeV protons from the CERN SPS with secondary pions and kaons focused with a magnetic horn into a 900 m decay pipe. The expected spectrum is much higher energy than NuMI and optimized to detect the appearance of ν_τ events. Since there are almost no intrinsic ν_τ's in the beam, a near detector is not

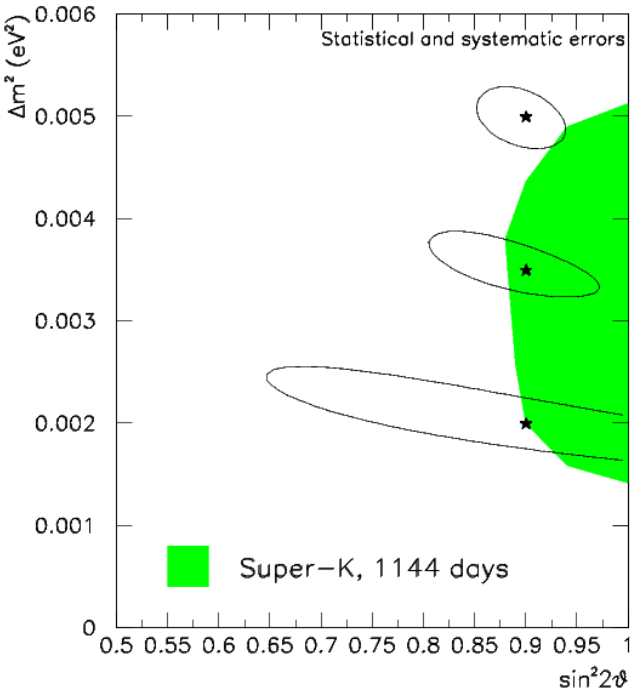

Figure 15. The plot shows the 90% CL allowed regions from the fits to reconstructed CC energy distributions for 10 kton-years of MINOS data. These distributions are generated with specific oscillation parameters as indicated by the stars.

planned and an oscillation signal can be confirmed with only a few events. The OPERA experiment uses emulsion bricks interspersed with electronic trackers. The emulsion bricks are composed of 1mm thick lead plates followed by 300 micron double sided emulsion plates stacked together in 56 layer units that weigh 8.3 kg and are 10 X_0 long. Tau neutrino events are identified by observed τ-decays in the emulsion. The goal is to expose 1.5 ktons of these hybrid emulsion bricks for 5 years and obtain a few dozen appearance ν_τ events over a very low background, ~ 0.5 events. The other CNGS experiment is ICARUS, which is to use a 5 ktons of liquid argon instrumented as a time projection chamber. If successful, this experiment will be a true electronic bubble chamber with excellent detection and identification properties for all species of neutrino events. Both ICARUS and OPERA as designed should

have sensitivity over the full Super-K allowed region, decreasing in the lower $\Delta m^2 = 10^{-3}$ region.

8 Oscillation Experiments at High Δm^2 - The LSND Region

Using data collected between 1993 to 1998 using the 800 MeV proton beam from the LANSCE accelerator, the LSND (Liquid Scintillation Neutrino Detector) observed an excess of $\overline{\nu}_e$ events in beam starting without this component. The beam was produced from stopping π^+'s made from interactions of the 800 MeV protons in the beam stop. (Almost all π^-'s are captured and do not decay.) The π^+ decay chain produced ν_μ, ν_e, and $\overline{\nu}_\mu$ neutrinos, but no $\overline{\nu}_e$ neutrinos. The claimed oscillation signal was then associated with an excess of $\overline{\nu}_e$ events tentatively from $\overline{\nu}_\mu \rightarrow \overline{\nu}_e$ oscillations:

$$\begin{aligned} \pi &\rightarrow \mu^+ \nu_\mu \\ &\hookrightarrow e^+ \nu_e \overline{\nu}_\mu \\ \textit{if oscillations} \qquad &\hookrightarrow \overline{\nu}_e + p \rightarrow e^+ + n \ . \end{aligned}$$

The LSND detector has 167 tons of liquid scintillator in a cylindrical tank viewed by 1280 8-inch photomultiplier tubes on the outer surface looking inward, and is located 30 m from the beam stop. The $\overline{\nu}_e$ signal gives an outgoing positron whose scintillation light is observed and a neutron, which also gives a 2.2 MeV γ after capturing on a free proton in the tank. The capture γ in a candidate event is required to have the proper time, energy, and spatial measurement using a likelihood technique. With this setup, $\overline{\nu}_\mu \rightarrow \overline{\nu}_e$ oscillations are probed for $\overline{\nu}_\mu$ energies between 20 and 55 MeV. The final LSND results have been published,[30] and indicate an excess of $87.9 \pm 22.4 \pm 6.0$ $\overline{\nu}_e$ events corresponding to a 3.3σ $0.264 \pm 0.067 \pm 0.045$ % oscillation probability. Fig. 16 shows the energy distribution of the signal and background events.

The KARMEN II experiment has also investigated this region of oscillation parameter space although with less sensitivity than LSND. KARMEN uses a pulsed 800 MeV proton beam from the Rutherford ISIS accelerator. The beam is again a beam-stop pion decay at rest beam located 17.6 m from the KARMEN detector. The detector used 56 tons of liquid scintillator contained in 512 modules that were Gd doped to have better neutron capture efficiency. Overall, the KARMEN II experiment probes the upper Δm^2 part of the LSND signal range. The data sample is ten times smaller than LSND due to lower neutrino flux and less detector mass; the detector is located closer to the neutrino source. For their final results, KARMEN II observed

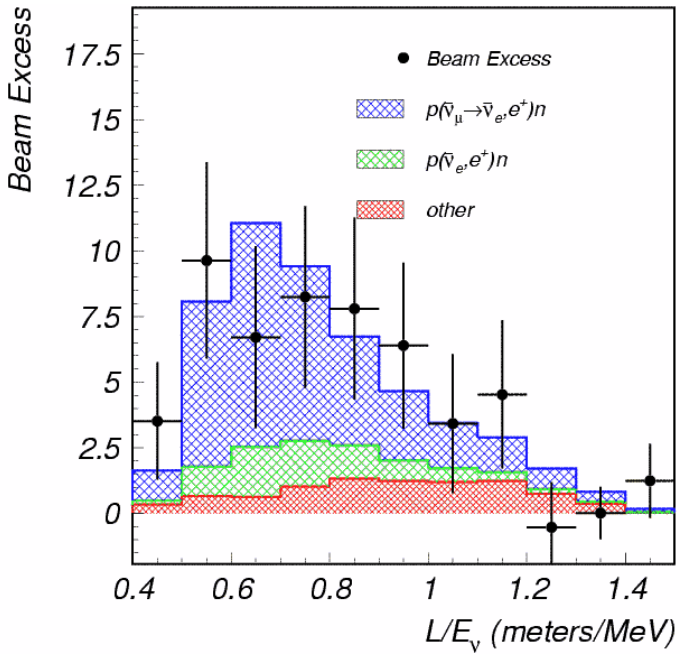

Figure 16. The energy distribution of the LSND excess events. The bottom cross hatched areas gives the non-electron neutrino background, the next area the electron neutrino background, and the top area gives the best fit oscillation hypothesis at high Δm^2.

no excess of $\overline{\nu}_e$ events; 11 events observed with 12.3 ± 0.6 expected from background sources. Church *et al.*[31] have done a joint analysis of the LSND and KARMEN II results. They find that the two experiments are incompatible at the 36% level and have mapped out the common parameter space shown in Fig. 17. It is clear from this analysis that another experiment is needed to make a definitive statement about the LSND anomaly.

The MiniBooNE experiment is designed to make a definitive investigation of $\nu_\mu \rightarrow \nu_e$ oscillations in the LSND signal region. The experiment uses 8 GeV protons from the Fermilab booster synchrotron to produce a wide-band neutrino beam with a mean energy of about 1 GeV. The protons hit a Be target, and secondary pions and kaons are focused with a magnetic horn into a 50 long decay pipe. A spherical detector, 12 m in diameter, is located 500 m away. The detector is filled with 800 tons of mineral oil (445 tons in the fiducial volume) and instrumented with ∼1280 8-inch phototubes on the

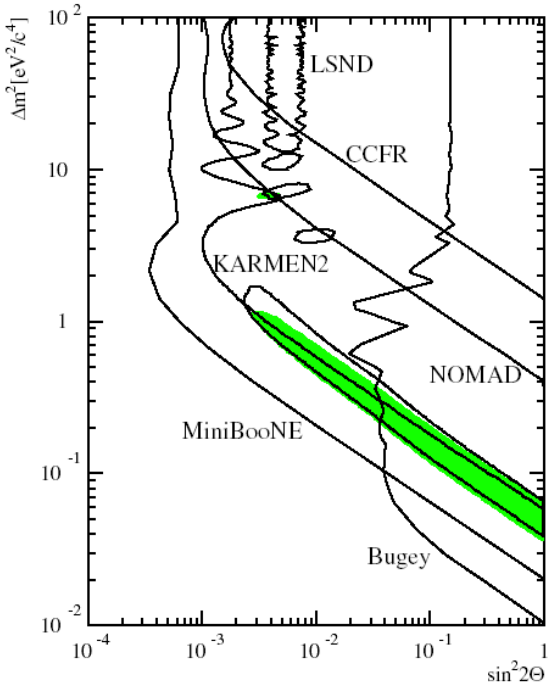

Figure 17. Parameter regions deduced from the combined LSND and KARMEN data (grey areas) compared with existing limits of experiments (Bugey $\overline{\nu}_e \to \overline{\nu}_x$, CCFR $\nu_\mu \to \nu_e$, and NOMAD $\nu_\mu \to \nu_e$) and the predicted sensitivity of the future MiniBooNE experiment.

surface looking inward. (An isolated veto region covers the outside radius and uses another 240 phototubes.)

The MiniBooNE beam is a very pure ν_μ beam with only a small contamination of ν_e's from K_{e3} and μ decay. With two years of running, MiniBooNE expects to record hundreds of thousands of ν_μ CC events over a background of a few thousand ν_e and mis-identified events. The distance and energy are matched to the LSND signal region with an $L/E \sim 1$ m/MeV and, if the LSND signal is true, MiniBooNE should see hundreds to thousands of excess events. There are experimental handles to allow the size and shape of all backgrounds to be determined from data. Two features have also been instrumented to allow further background checks: 1) the decay has an inter-

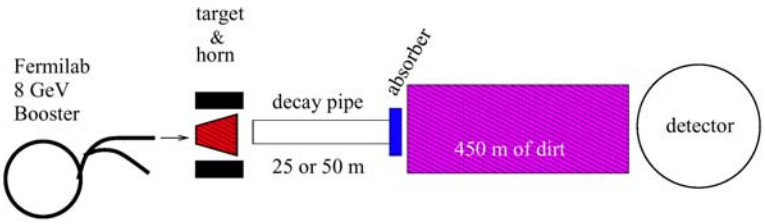

Figure 18. Schematic diagram of the MiniBooNE beamline.

mediate absorber that can be used to shorten the decay pipe to 25 m and 2) a narrow channel off the decay pipe has been instrumented to detect wide-angle muons from K decay.

With 5×10^{20} booster protons ($\sim$2 year of running), MiniBooNE will completely include or exclude the entire LSND signal region at the 5σ level. For this data sample, Δm^2 can be measured to 0.1 eV^2 and $\sin^2 2\theta$ to 10-60%. The MiniBooNE sensitivity at the 90% CL level is shown in Fig. 17. If a signal is observed in MiniBooNE, then the next step would be to move toward the two detector experiment, BooNE, by adding a second detector at an appropriate distance. For high $\Delta m^2 \approx 1$ eV^2, the second detector should be closer at about 250 m; for $\Delta m^2 \approx 0.3$ eV^2, the new detector should be at the Fermilab site boundary, 2000 m. With the BooNE two detector setup, Δm^2 can be measured to 0.014 eV^2 and $\sin^2 2\theta$ to $<$10 %.

9 Neutrino Oscillation Summary, Interpretations and Future Prospects

The next steps for neutrino oscillation studies will be driven by the near term results from the current set of experiments. If MiniBooNE sees a $\nu_\mu \rightarrow \nu_e$ oscillation signal, then new experiments will be needed to investigate oscillations at relatively high Δm^2. At least four mass eigenstates are needed to explain the solar, atmospheric, and LSND results implying the existence of sterile neutrinos or CPT violation (see later).

If MiniBooNE refutes LSND, then MINOS(CNGS) will test the oscillation phenomenology and measure the parameters with better precision for the atmospheric oscillation region. After fixing the atmospheric oscillation phenomenology, the next step will be to determine the size of $\nu_\mu \rightarrow \nu_e$ transitions in the atmospheric Δm^2 region. This transition is the path to measuring the third mixing angle θ_{13}, to investigating matter effects and the mass hierar-

chy of neutrinos, and to making searches for CP violation in the neutrino sector. The MINOS/CNGS experiments will extend the search for $\nu_\mu \rightarrow \nu_e$ oscillations by about a factor of two relative to the CHOOZ limit.

A MINOS off-axis experiment[33] or a future experiment at the Japanese Hadron Facility (JHF)[34] could extend this search another factor of ten in sensitivity; both options are being actively investigated. If, with these new experiments, $\nu_\mu \rightarrow \nu_e$ oscillations are not observed, then it will be necessary to design a new experimental facility with the capability to measure $\sin^2 2\theta_{13}$ down to the 0.001 level. The new facility may be a long baseline, very high intensity neutrino facility ("Superbeam")[35] or a neutrino beam from a high intensity muon storage ring facility ("ν-Factory")[36]; again both of these options are being considered. If $\nu_\mu \rightarrow \nu_e$ oscillations are observed at any point, then a program of experiments to measure CP violation and matter effects should be instituted.

In the scenario where MiniBooNE confirms LSND, a fourth (or more) sterile neutrino type might be included to explain the three independent Δm^2 ranges for solar, atmospheric, and LSND. The fourth neutrino can be added in a number of ways as shown in Fig. 19. In the 3+1 model, the fourth (mainly sterile) neutrino is either lighter or heavier than all the others by Δm^2_{LSND} and has small (~5%) admixtures of the ν_μ, ν_e, and ν_τ. The LSND $\nu_\mu \rightarrow \nu_e$ oscillations occur by mixing through the sterile neutrino. The solar oscillations are ν_e oscillations to a 50%/50% mixture of ν_μ and ν_τ. An example of the flavor composition for a 3+1 model is given by

$$\begin{aligned}
\nu_e &= +0.85\nu_1 + 0.51\nu_2 \\
\nu_\mu &= -0.36\nu_1 + 0.60\nu_2 + 0.71\nu_3 \\
\nu_\tau &= +0.36\nu_1 - 0.60\nu_2 + 0.71\nu_3
\end{aligned}$$

In the 2+2 model, the four mass eigenstates are put together in two pairs corresponding to the atmospheric and solar Δm^2 values; these two pairs are then split Δm^2_{LSND} as shown in Fig. 19. In this model, atmospheric and solar (or both) can have oscillation fractions to the sterile neutrinos but the fractions must add to one, $f_{solar} + f_{atmos} = 1$. The current Super-K atmospheric measurements limit $f_{atmos} < 0.25$ at 90% CL and the SNO/Super-K solar measurements limit $f_{solar} < 0.40$ at 90% CL. So, this model is still possible, but only at the edges of probability and might have to be modified to include more than one sterile neutrino to be viable. Maltoni *et al.*[37] have made a global analysis of the solar, atmospheric, LSND, Karmen, and reactor data for the 3+1 and 2+2 models; the allowed regions from their fits is shown in Fig. 20.

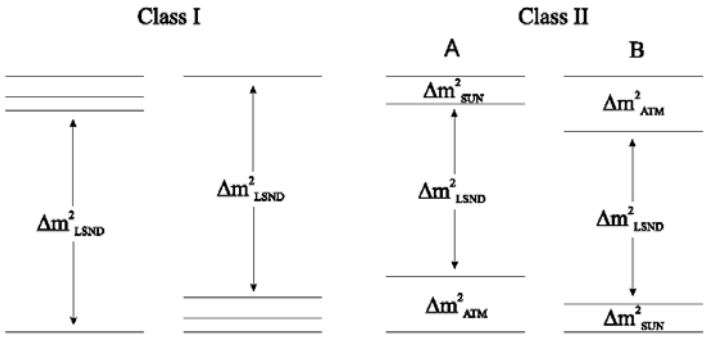

Figure 19. Different types of four family neutrino mass hierarchies including the $3+1$ (left) and $2+2$ (right).

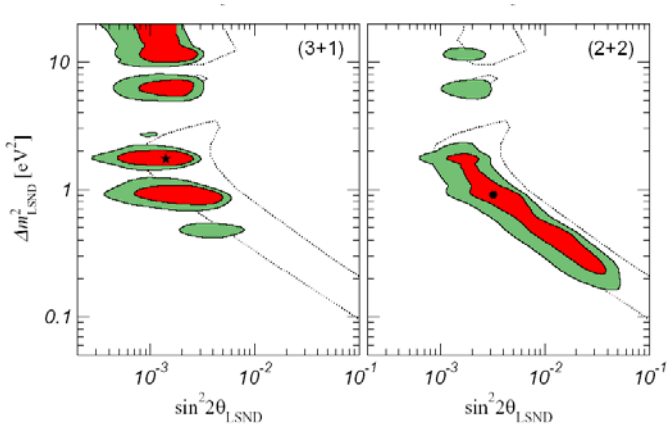

Figure 20. Global combined fits [37] of current neutrino oscillation data. The allowed areas correspond to 90% and 99% CL regions associated with the fit with the best fit points marked by the star and circle. The dotted line is the 99% CL region from the LSND data alone.

Another idea to explain the three oscillation signals invokes CPT violation where the masses for a neutrino and its antineutrino partner can be different. A crucial point is that the LSND signal is for antineutrino oscillations, $\overline{\nu}_\mu \to \overline{\nu}_e$, and the solar neutrino deficit is for electron neutrinos disappearing, $\nu_\mu \to$

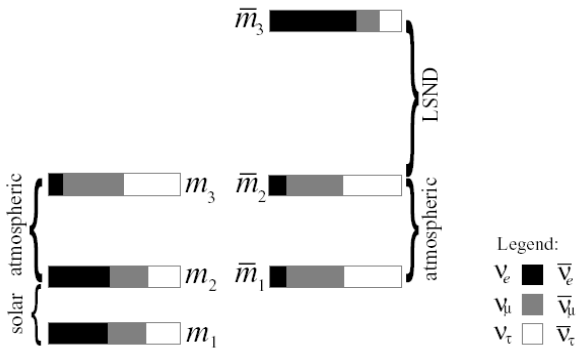

Figure 21. Example CPT violating mass spectrum that is able to explain the LSND, atmospheric, and solar neutrino evidence. The mass of the eigenstate is represented by the height in the figure and the flavor components of the state by the shading.

ν_x. The CPT violation model put forward by G. Barenboim *et al.*[38] can explain all current data by allowing the antineutrinos to have larger Δm^2 values than the neutrinos as shown in Fig. 21. This model will be tested soon by the Kamland and MiniBooNE experiments. Kamland is looking for the disappearance of reactor antineutrinos in the solar Δm^2 range; with this model they will see no oscillation signal. MiniBooNE can run with both ν_μ and $\overline{\nu}_\mu$ beams; for this model, MiniBooNE will only see an oscillation signal for $\overline{\nu}_\mu$'s.

Even if MiniBooNE refutes LSND, there are many more measurements that need to be made in order to understand the neutrino mixing matrix, neutrino mass hierarchy, and the possibility of CP violation. For a three generation model, the mixing is given by

$$\begin{pmatrix} \nu_e \\ \nu_\mu \\ \nu_\tau \end{pmatrix} = \begin{pmatrix} 1 & & \\ & c_{23} & s_{23} \\ & -s_{23} & c_{23} \end{pmatrix} \begin{pmatrix} c_{13} & & s_{13}e^{i\delta} \\ & 1 & \\ -s_{13}e^{i\delta} & & c_{13} \end{pmatrix} \begin{pmatrix} c_{12} & s_{12} & \\ -s_{12} & c_{12} & \\ & & 1 \end{pmatrix} \begin{pmatrix} \nu_1 \\ \nu_2 \\ \nu_3 \end{pmatrix}$$

Current measurements will determine θ_{23} and θ_{12} with some precision. Future measurements need to accurately determine the two Δm^2 values; the sign of Δm^2_{23} in order to fix the mass hierarchy; and the size of the missing angle, θ_{13}. If θ_{13} is large enough, then the measurement of the CP violation phase δ may be feasible by comparing $\nu_\mu \to \nu_e$ and $\overline{\nu}_\mu \to \overline{\nu}_e$ oscillations. For these type of studies, a ν-factory beam[36] from a high intensity muon storage ring

(Fig. 22) would be ideal. The storage ring would provide a super-intense neutrino beam with a wide (but well understood) range of energies. The produced neutrino beam is mixed flavor with electron antineutrinos and muon neutrinos for positive muon decay and the opposite for negative muon decay.

$$\mu^- \rightarrow e^- + \nu_\mu + \overline{\nu}_e$$
$$\mu^+ \rightarrow e^+ + \overline{\nu}_\mu + \nu_e$$

In addition, the beam is highly collimated allowing very long baseline experiments in the few thousand kilometer range. By measuring $\nu_e \rightarrow \nu_\mu$ oscillations, the signal becomes a search for wrong-sign muon events, which are easy to identify and have reduced backgrounds. With this technique, it has been estimated[36] that $\sin^2 2\theta_{13}$ could be measured with a value as low as 0.001 for an exposure corresponding to 2×10^{20} μ-decays. These studies have also looked at sensitivities for measuring matter and CP violation effects as displayed in Fig. 23.

As a final note, it is interesting to compare the mixings of quarks and neutrinos and speculate on this phenomenology. For the quarks, the mixing is given by

$$\begin{pmatrix} d' \\ s' \\ b' \end{pmatrix} = \begin{pmatrix} 0.97 & 0.22 & 0.003e^{i\delta} \\ -0.22 & 0.97 & 0.04 \\ 0.01 & -0.04 & 0.999 \end{pmatrix} \begin{pmatrix} d \\ s \\ b \end{pmatrix}$$

and the neutrino mixing is given approximately by

$$\begin{pmatrix} \nu_e \\ \nu_\mu \\ \nu_\tau \end{pmatrix} = \begin{pmatrix} 0.7 & 0.7 & < 0.2e^{i\delta} \\ -0.5 & 0.5 & 0.7 \\ 0.5 & -0.5 & 0.7 \end{pmatrix} \begin{pmatrix} \nu_1 \\ \nu_2 \\ \nu_3 \end{pmatrix}.$$

The quark mixing has little mixing especially between d and b quarks; the neutrinos readily mix among all species. Due to this large mixing in the neutrino sector relative to quarks, speculations have been put forward to explain the baryon asymmetry in the universe through a lepton number violation using CP or CPT violation in the lepton sector. This possibility, along with the implications of neutrino mass and oscillations for cosmology, astrophysics, and Standard Model, makes this a very interesting time for neutrino physics.

References

1. F. Reines and C.L. Cowan, *Phys.Rev.* **92** 830 (1953).
2. G. Danby *et al.,Phys. Rev. Lett.* **9**, 36 (1962).

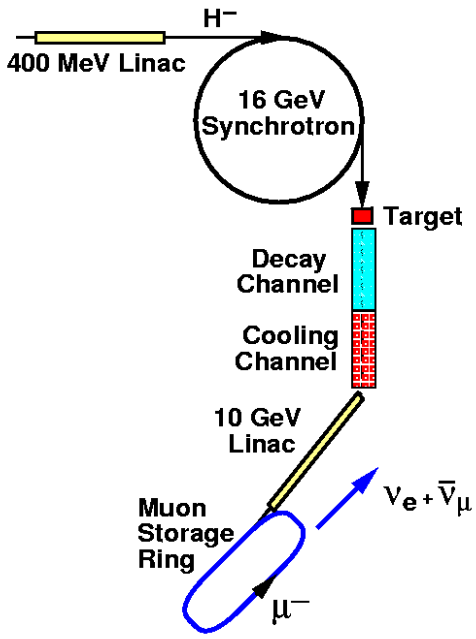

Figure 22. Schematic layout for a muon storage ring facility producing a ν-factory neutrino beam.

3. K. Kodama *et al.,Phys. Lett.* B **504**, 218 (2001).
4. J.M.Conrad, M.H. Shaevitz, and T. Bolton , *Rev. Mod. Phys.* **70**, 1341 (1998).
5. P. Langacker *et al., Rev. Mod. Phys.* **64**, 87 (1991).
6. K.S. McFarland, D. Naples *et al., Phys. Rev. Lett.* **75**, 3993 (1995).
7. C.H. Llewellyn Smith, *Nucl. Phys.* B **228**, 205 (1983).
8. E.A. Paschos and L. Wolfenstein, *Phys. Rev.* D **7**, 91 (1973).
9. G.P. Zeller, *et al., Phys. Rev. Lett.* **88**, 91802 (2002).
10. K.S. McFarland, *et al., Eur. Phys. J.* **C1**, 509 (1998).
11. S. Davidson, *et al.,* hep-ph/0112302, March, 2002.
12. D. Bardin and V.A. Dokuchaeva, *JINR-E2-86_260* (1986); D. Bardin, *et al., Comp. Phys. Commun.* **133**, 229 (2001).
13. LEP/SLD Electroweak Working Group, hep-ex/0111221, with updates from M. Grünewald (private communication) for fits without neutrino

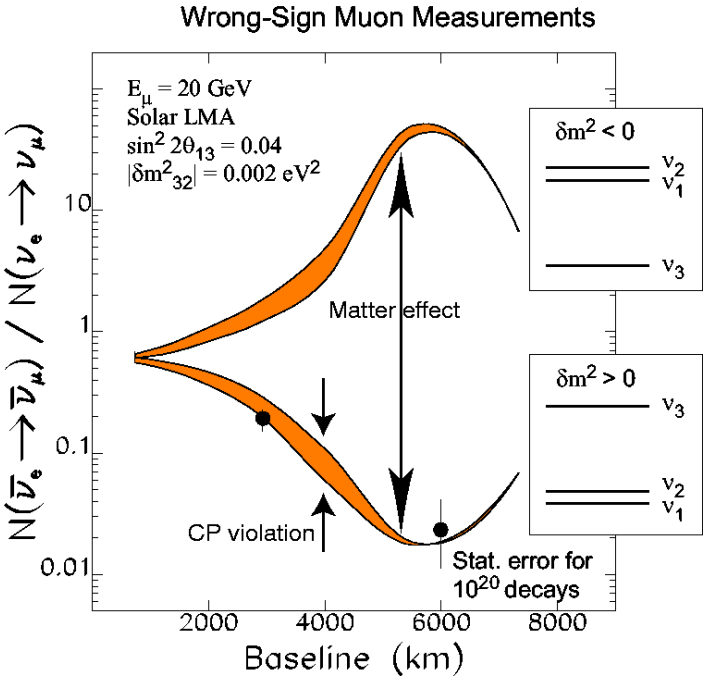

Figure 23. Ratio of electron neutrino to antineutrino oscillations versus baseline distance for a ν-factory experiment with 2×10^{20} 20 GeV muon decays. The two curves correspond to different signs of Δm^2 and the width of the curves reflect CP violation effects. The two data points give estimates of the experimental error in measuring the ratio.

data and results posted at http://lepewwg.web.cern.ch/LEPEWWG/.

14. G.A. Miller and A.W. Thomas, hep-ex/0204007, April 2002.
15. G.P. Zeller *et al.* (NuTeV Collaboration), hep-ex/0203004, March 2002.
16. E.N. Rodionov, *et al.*, *Mod. Phys. Lett.,* **A9**, 1799 (1994); F. Cao *et al.*, *Phys. Rev.* **C62**, 015203 (2000).
17. K.S. Babu and J.C. Pati, hep-ph/0203039, March 2002.
18. C. Giunti and M. Laveder, hep-ph/0202152, Feb. 2002.
19. See KATRIN Homepage at http://ik1au1.fzk.de/˜katrin/.
20. K. Assamagan *et al., Phys. Rev.* D **53**, 6065 (1996).
21. Aleph Collaboration , *Eur. Phys. J.* **C2**, 395 (1998).
22. L. Baudis *et al., Phys. Rev. Lett.* **83** 41 (1999); (Part of this group

has also reported positive evidence of $\langle m \rangle$ = (0.11-0.56) eV at 95% CL in H.V. Klapdor-Kleingrothaus *et al., Modern Physics Letters* **A16** 2409 (2001)).
23. Q.R. Ahmad, *et al.,* nucl-ex/0204008, April, 2002.
24. Q.R. Ahmad, *et al.,* nucl-ex/0204009, April, 2002.
25. T.K. Gaisser and M. Honda, hep-ph/0203272, March, 2002.
26. M. Appolonio, *et al., Phys. Lett.* B **466**, 415 (1999).
27. S. Fukuda, *et al., Phys. Rev. Lett.* **85**, 3999 (2000).
28. S.H. Ahn, *et al., Phys. Lett.* B **511**, 178 (2001); J.E. Hill, *et al.,*hep-ex/0110034; C.K. Jung in Proceedings of the Lepton-Photon 2001 Conf.; (http://www.lp01.infn.it/proceedings/jung.pdf) .
29. See MINOS web site at: http://www-numi.fnal.gov/forscientists.html and http://www-numi.fnal.gov/blessed/index.html
30. A. Aguilar, *et al., Phys. Rev.* D **64**, 112007 (2001).
31. E.D. Church, *et al.,*hep-ex/0203023, March,2002.
32. A.O. Bazarko *et al.*, *Nucl. Phys.* **B**(Proc. Suppl.)**91**, 210 (2001); MiniBooNE Homepage at http://www-boone.fnal.gov/ .
33. "Letter of Intent to Build an Offaxis Detector for the NuMI Neutrino Beam", D. Ayres *et al.,* June, 2002, available at http://www-numi.fnal.gov/fnal_minos/new_initiatives/loi.html .
34. Y. Itow, *et al.,*hep-ex/0106019, June,2001.
35. V. Barger, *et al.,*hep-ex/0103052, March,2001.
36. C. Albright, *et al.,*hep-ex/0008064, April, 2000.
37. M. Maltoni, *et al., Phys. Rev.* D **65**, 093004 (2002).
38. G. Barenboim, *et al.,*hep-ph0108199, August, 2001; G. Barenboim, *et al.,*hep-ph0201080, January, 2002.